

PAPER • OPEN ACCESS

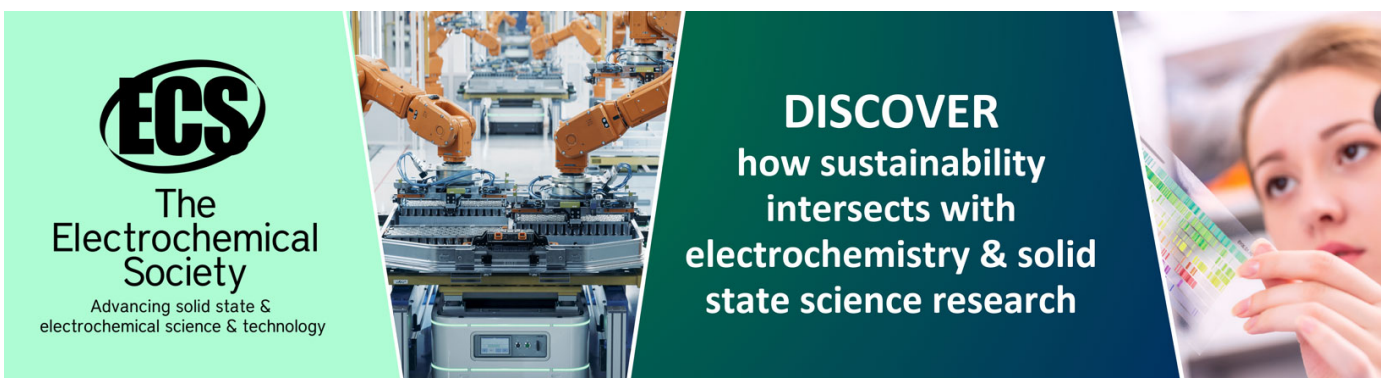
Microplasma assisted synthesis of gold nanoparticle/graphene oxide nanocomposites and their potential application in SERS sensing

To cite this article: Daye Sun *et al* 2019 *Nanotechnology* **30** 455603

View the [article online](#) for updates and enhancements.

You may also like

- [Facile synthesis and characterisations of cobalt ferrite-silver-graphene oxide nanocomposite in enhancing electrochemical response capacity](#)
Van-Tuan Hoang, Nguyen Le Nhat Trang, Dao Thi Nguyet Nga et al.
- [Bio-green synthesis of Ag-GO, Au-GO and Ag-Au-GO nanocomposites using *Azadirachta indica*: its application in SERS and cell viability](#)
K Hareesh, J F Williams, N A Dhole et al.
- [Structural, optical, magnetic properties and visible light photocatalytic activity of BiFeO₃/graphene oxide nanocomposites](#)
Fatemeh Noori and Ahmad Gholizadeh



ECS
The
Electrochemical
Society
Advancing solid state &
electrochemical science & technology

DISCOVER
how sustainability
intersects with
electrochemistry & solid
state science research

Microplasma assisted synthesis of gold nanoparticle/graphene oxide nanocomposites and their potential application in SERS sensing

Daye Sun¹ , Miao Tang², Li Zhang³ , Brian G Falzon¹ ,
Dilli Babu Padmanaban⁴, Davide Mariotti⁴ , Paul Maguire⁴ ,
Heping Xu² , Mei Chen² and Dan Sun¹ 

¹ Advanced Composites Research Group (ACRG), School of Mechanical and Aerospace Engineering, Queen's University, Belfast BT9 5AH, United Kingdom

² The Wellcome-Wolfson Institute of Experimental Medicine, School of Medicine, Dentistry and Biomedical Sciences, Queen's University Belfast BT9 7BL, United Kingdom

³ Research Center for Nano-Biomaterials, Analytical & Testing Center, Sichuan University, Chengdu 610065, People's Republic of China

⁴ Nanotechnology and Integrated Bioengineering Centre, Ulster University, Co Antrim BT37 OQB, United Kingdom

E-mail: d.sun@qub.ac.uk

Received 28 March 2019, revised 3 June 2019

Accepted for publication 17 June 2019

Published 27 August 2019



CrossMark

Abstract

This is the first study on the deployment of direct current atmospheric pressure microplasma technique for the single step synthesis of gold nanoparticle/graphene oxide (AuNP/GO) nanocomposites. The nanocomposites were characterized using ultraviolet–visible spectroscopy (UV–vis), x-ray diffraction and x-ray photoelectron spectroscopy and their formation mechanisms have been discussed in detail. Our AuNP/GO nanocomposites are highly biocompatible and have demonstrated surface enhanced Raman scattering (SERS) properties as compared to pure AuNPs and pure GO. Their potential as SERS substrate has been further demonstrated using probe molecules (methylene blue) at different concentrations.

Supplementary material for this article is available [online](#)

Keywords: gold nanoparticles, graphene oxide, atmospheric pressure microplasma, surface enhanced Raman scattering, biosensing

(Some figures may appear in colour only in the online journal)

Introduction

Atmospheric pressure microplasma (APM) operates at room temperature under non-thermal equilibrium conditions with high electron temperature (e.g. 10^4 K) [1, 2]. When in contact with aqueous solution, APM can lead to dynamic production of highly reactive species including solvated electrons, radicals (e.g. OH^\bullet , H^\bullet , and O^\bullet , etc.), ions (e.g. OH^- and H^+), and H_2O_2 [3, 4]. These species can interact with metal salt precursors within the aqueous

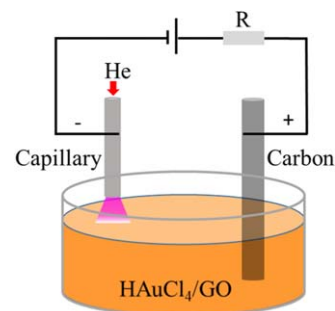
solution via different reaction pathways, initiating the reduction of metal ions [5–7]. As a result, APM-liquid interaction has become an emerging technology for the synthesis of various metal based nanoparticles (NPs) such as AgNPs, AuNPs, Cu_2O NPs, Co_3O_4 , Fe_3O_4 NPs, and alloyed $\text{Au}_x\text{Ag}_{1-x}$ NPs [6–12]. The unique advantage of the APM synthetic approach is its ability to create highly charged NP surfaces within minutes and enable the stabilisation of NPs in aqueous based solutions without the need for surfactants or ligand coating.



In recent years, APM based nanomaterials synthesis has been expanded further towards the fabrication of nano-composite systems. By exposing aqueous mixture of metal salt precursors and polymers to high doses of plasma induced reactive species, we have successfully achieved one-step synthesis of a number of multifunctional nanocomposites such as AuNP/PEDOT: PSS for potential fuel cell electro-catalyst, thermos-responsive $\text{Fe}_3\text{O}_4/\text{poly}$ (N-isopropylacrylamide), and AuAg NP/PVA hydrogel nanocomposites for potential bioapplications [13–15]. We have also developed the rapid and green APM synthesis process for the fabrication of AuNP decorated carbon nanotubes with enhanced photothermal conversion capability [16]. These preliminary results highlight the exciting possibility of using APM to synthesize a wide range of advanced nanocomposites for functional applications.

Graphene oxide (GO), one of the graphene derivatives, is a two-dimensional (2D) sheet with a sp^2 -hybridized carbon atoms packed into a honeycomb lattice [17]. While retaining the unique structure and excellent mechanical properties of graphene, GO is rich in surface functional groups (e.g. $-\text{OH}$, $-\text{C}-\text{O}-$ and $-\text{COOH}$), which promote the cell adhesion and biocompatibility [18, 19]. Functional metallic NPs, in particular gold NPs (AuNPs), when incorporated into GO, can form multifunctional nanocomposites for many applications such as drug delivery, tissue engineering, electrocatalysis [20–22]. AuNP/GO nanocomposites are also of particular interest for surface enhanced Raman scattering (SERS) sensing [23]. In SERS sensing, AuNPs with localized surface plasmon resonance property could lead to a much higher Raman signal enhancement through the electromagnetic mechanism (EM) [24]. GO on the other hand, can offer enhanced Raman signal through a chemical mechanism (CM) due to the electron transfer between the analyte and the graphene structures [25]. AuNPs/GO nanocomposites can fully deploy both mechanisms, leading to a much enhanced SERS capability [26]. To date, AuNP/GO nanocomposites with SERS activities have been reported in a number of SERS related applications, such as detection of aromatic molecules and biomolecules, intercellular imaging, and cancer diagnostics [20, 27–32]. Some of the synthetic routes of AuNP/GO nanocomposites reported for SERS based applications have been summarized in table 1. Although traditional wet chemistry based synthesis techniques (e.g. *in situ* chemical reduction [30, 33, 34], self-assembling [31, 35–38], and electrochemical deposition [39]) have been commonly used, most of these approaches require elevated temperatures, long processing time (hours), and/or multiple reaction steps/cleansing procedures. Photo-reduction process has also been reported for the synthesis of AuNP/rGO [40], however, the long exposure to UV-irradiation may be potentially hazardous to human [41].

In this work, we demonstrated the first use of a direct current (DC) APM for the one-step synthesis of AuNP/GO nanocomposites. An in-depth understanding has been developed into the interfacial interactions between AuNP and GO during the APM assisted synthesis process and the formation mechanism of AuNP/GO nanocomposites under the plasma



Scheme 1. APM set-up used in the present work.

induced chemistry has been elucidated in detail. The resulting AuNP/GO nanocomposites have been evaluated for their biocompatibility and their potential as SERS substrate has been demonstrated using a model probe molecule methylene blue (MB).

Experiment section

APM set-up

The APM set-up deployed in this study is shown in scheme 1. The cathode consists of a hollow stainless-steel capillary with an inner diameter of $250\ \mu\text{m}$, and the anode is a conductive carbon rod which is immersed in the solution. The two electrodes were vertically placed with a distance of $\sim 2\ \text{cm}$ in between. The capillary is placed $\sim 1\ \text{mm}$ above the liquid surface, through which helium (He) gas was supplied (25 SCCM). The plasma can be ignited at $\sim 2\ \text{kV}$ and all samples were treated at a constant current of $5\ \text{mA}$ for $10\ \text{min}$ without stirring the solutions.

The preparation of AuNP/GO nanocomposites

GO aqueous solution (Graphene Laboratories Inc., $50\ \text{mg}\ \text{ml}^{-1}$) was mixed with HAuCl_4 (Sigma-Aldrich) aqueous solution to obtain aqueous HAuCl_4/GO mixtures with constant GO concentration ($0.5\ \text{mg}\ \text{ml}^{-1}$) and varying HAuCl_4 concentrations ($2.5\ \mu\text{M}$, $0.1\ \text{mM}$, and $0.2\ \text{mM}$). The resulting mixtures were settled for $10\ \text{min}$ before APM treatment. The samples after APM treatment were named as $2.5\ \mu\text{M}$ AuNP/GO, $0.1\ \text{mM}$ AuNP/GO, and $0.2\ \text{mM}$ AuNP/GO, respectively. All samples were collected and stored in glass vials for further analysis (see figure S1, available online at stacks.iop.org/NANO/30/455603/mmedia in supporting information).

Characterization

The optical properties of the samples were analysed using ultraviolet–visible (UV–vis) spectroscopy (Cary 60 UV–vis, Agilent Technologies). Transmission electron microscopy (TEM) analysis was carried out using a Philips Tecnai F20D transmission electron microscope, and size of the AuNPs within the nanocomposite was obtained by analysing 150 NPs using ‘ImageJ’ software. The diameter was measured for

Table 1. Au-graphene nanocomposites with enhanced SERS for biomolecule detection applications.

Method	Platform	Specified AuNP shapes	Interlayers	Reducing agent	Probe molecules	Applications	References
<i>In situ</i> chemical reduction	AuNP/GO	Spheres	N/A	Tyrosine	Malachite green (MG)	SERS	[30]
	AuNP/rGO	N/A	Polyvinylpyrrolidone	Ascorbic acid	NBA	SERS	[33]
	AuNP/GO	N/A	N/A	Sodium citrate	Rhodamine 6 G (R6G)	SERS	[34]
Self-assembling	AuNP/rGO	Rods	Polyvinylpyrrolidone	Sodium borohydride	Crystal violet (CV), neutral red (NR), trypan blue (TB) and ponceau S (PS)	SERS	[31]
	AuNP/GO						
	AuNP/GO						
ω	AuNP/GO	N/A	2-Mercaptopyridine	Sodium borohydride	Rh6G	SERS	[36]
		Popcorns	Thionyl chloride and cysteamine	Sodium citrate and sodium borohydride	Rh6G, HIV DNA, and methicillin resistant staphylococcus aureus (MRSA) bacteria	SERS	[38]
		N/A	2-Mercaptopyridine	Sodium citrate	P-aminothiophenol (PATP)	SERS and catalysis	[37]
Electrochemical UV-irradiation	AuNP/rGO	N/A	N/A	N/A	Rhodamine B (RhB)	SERS	[39]
	AuNP/GO	N/A	N/A	N/A	Crystal Violet (CV) and flavin adenine dinucleotide (FAD)	SERS and electro-chemical reactions	[40]

spherical NPs, while for NPs with other morphologies, the longest dimension was measured. X-ray powder diffraction (XRD) patterns of the samples were carried out using a PANalytical X'PERT Pro MPD machine, while the XRD pattern were referred to the JCPDS card. X-ray photoelectron spectroscopy (XPS) was conducted using Kratos Axis Ultra XPS system (monochromatic Al $K\alpha$ x-rays, 1486 eV) at 10 mA current, 15 kV voltage under 1×10^{-9} mbar of pressure. The XPS samples were prepared by drop-casting aqueous sample solutions on intrinsic silicon wafer, followed by drying thoroughly under room temperature. High-resolution XPS spectra (0.05 eV) including C 1s and Au 4f peaks of all samples were performed under a pass energy of 40 eV. The spectra were calibrated and normalized to the C 1s peak located at 284.5 eV and the data were analysed using an open source software CasaXPS. Samples for Raman test was prepared by drop-casting 100 μ l of each AuNP/GO aqueous solution on neat silicon wafer with a pre-fabricated 6 mm \times 6 mm well followed by drying under room temperature. Raman spectroscopy were performed using a 632 nm N_2-H_2 laser excitation Raman spectroscopy (LabRAM 300, Horiba, UK with a 632 nm source). The operating current and voltage of the laser is 7 mA and 3.7 kV, respectively. For all samples, a 1% filter of the output power (0.259 W) was chosen to avoid the surface damages of the materials. Measurements were repeated three times to ensure reproducibility.

SERS measurements

0.1 mM AuNP/GO was selected as a typical sample to evaluate the potential of our nanocomposites for SERS sensing applications. MB was used as model probe molecule. 1 ml of the 0.1 mM AuNP/GO aqueous solution was mixed with 1 ml MB of varying concentrations (2×10^{-1} , 2×10^{-2} , 2×10^{-3} , and 2×10^{-4} mg ml $^{-1}$), and the mixtures were settled for 30 min to allow thorough adsorption of the molecules. 100 μ l of each sample was drop-casted onto silicon wafer with a pre-fabricated 6 mm \times 6 mm well and dried thoroughly under ambient condition before conducting Raman scanning.

In vitro cytotoxicity test

The alamarBlueTM Cell Viability Reagent (ThermoFisher Scientific Inc., Gaithersburg, MD, USA) was used to determine the cytotoxicity of nanocomposites following the manufacturer's instruction. Immortalized human cervical cells, HeLa cells (ATCC[®] CCL2TM, Manassas, VA, USA) were cultured in Minimum Essential Medium (MEM, ThermoFisher Scientific Inc.) supplemented with 3.9 mM L-glutamine, 1.0 mM sodium pyruvate, 2.2 g l $^{-1}$ sodium bicarbonate and 10% fetal bovine serum (FBS) and maintained in a humidified atmosphere containing 5% CO $_2$ at 37 $^{\circ}$ C. HeLa cells were cultured until they reached approximately 80% confluency before preparing the plates for the cytotoxicity assay. Cells were seeded into Costar[®] 96-well assay plates (Costar 3904, Corning Inc., NY, USA) with different initial cell densities of 5×10^3 , 4×10^3 and

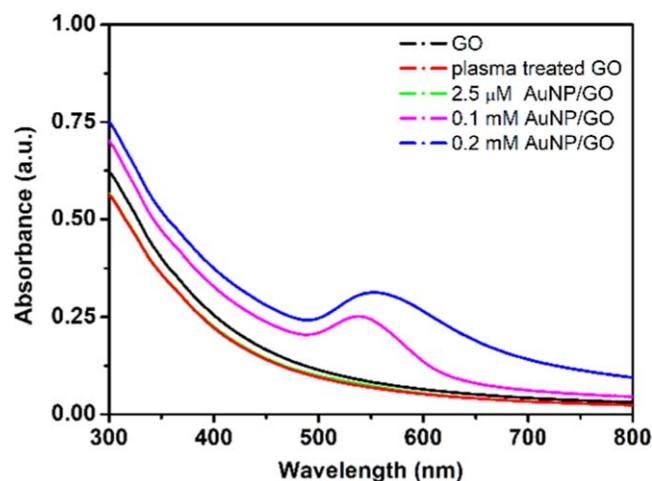


Figure 1. The UV-Vis spectra of GO, APM treated GO and AuNP/GO nanocomposites.

3×10^3 cells per well. The cells were cultured for 24 h to allow attachment to the wells. 100 μ l water suspension of tested materials, 0.1 mM AuNP, GO, or 0.1 mM AuNP/GO was mixed with 100 μ l 2X MEM supplemented with 10% FBS and 1% Primocin (ThermoFisher Scientific Inc.). For each well, the cultured medium was replaced with 200 μ l complete medium of tested materials. Cells were maintained in 37 $^{\circ}$ C incubator for 24 h, 48 h and 72 h, corresponding to the initial cell density of 5×10^3 , 4×10^3 , 3×10^3 cells per well, respectively. 100 μ l of autoclaved double-distilled water was used as no treatment control. After each time point, cells were washed twice with PBS. Complete medium containing 10% alamarBlue[®] solution was added and incubated in the 37 $^{\circ}$ C incubator for 2 h. After incubation, fluorescence was measured using a POLARstar[®] Glomax multidetection system (Promega, Southampton, UK) with excitation/emission wavelength at 544/590 nm. Cell viability was calculated by the relative ratio of fluorescence from test materials to control media.

Results and discussion

HAuCl $_4$ /GO mixtures showed immediate colour change when the samples were subjected to APM treatment (see figure S1 in supporting information). The optical properties of the APM treated samples are shown in figure 1. It can be seen that the UV-vis absorption spectrum of GO is insensitive to the APM treatment. However, in the presence of HAuCl $_4$, the UV-vis spectra of APM treated 0.1 mM HAuCl $_4$ /GO (0.1 mM AuNP/GO) and 0.2 mM HAuCl $_4$ /GO (0.2 mM AuNP/GO) mixtures both display a surface plasmon resonance (SPR) band typical of AuNPs (539 nm and 553 nm, respectively). The SPR peak wavelength is red shifted with increasing initial HAuCl $_4$ concentration (from 0.1 to 0.2 mM). This can be attributed to the larger AuNPs formed within samples containing higher HAuCl $_4$ concentration [42].

The presence of AuNP on GO was further confirmed by TEM analysis, see figure 2. Figure 2(A) shows a typical TEM

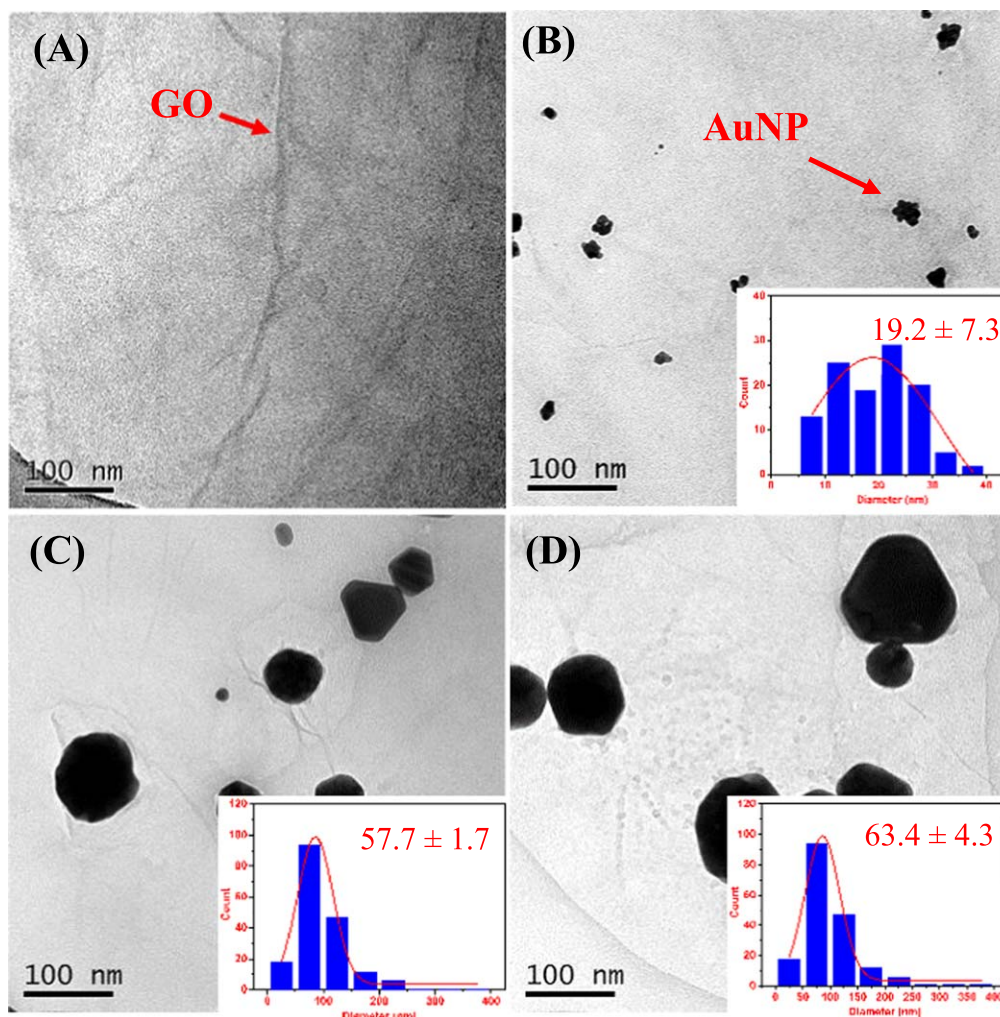


Figure 2. TEM micrographs of (a) GO, (b) $2.5 \mu\text{M}$ AuNP/GO, (c) 0.1 mM AuNP/GO, and (d) 0.2 mM AuNP/GO; (b)–(d) insets: size distribution of AuNPs within each sample.

image of GO sheets. AuNPs were found to be well dispersed on the surfaces of GO for the plasma treated samples, see figures 2(B)–(D). It can be seen that AuNPs are present in the $2.5 \mu\text{M}$ AuNP/GO sample, although no AuNP SPR band has been observed in its associated UV–vis spectrum in figure 1. This may be due to the number of NPs formed under very low initial HAuCl_4 is below the UV–vis detection limit [16]. The average NP size increased from $19.2 \pm 7.3 \text{ nm}$ to $63.4 \pm 4.3 \text{ nm}$ with increasing HAuCl_4 precursor concentration (figures 2(B)–(D) insets). This is consistent with the red shift of the SPR peak shown in UV–vis absorption spectra in figure 1. It is noteworthy that the AuNPs within the $2.5 \mu\text{M}$ AuNP/GO sample feature clusters of coalesced NPs with much smaller sizes (see also figure S2 in supporting information), in contrast to the well dispersed single AuNPs in 0.1 and 0.2 mM AuNP/GO samples.

It is also of interest to investigate if the GO within the nanocomposite structure has undergone any reduction reaction (e.g. formation of reduced GO) during the APM treatment. Figure 3 shows the XRD spectra of pure GO and APM treated GO. For pure GO, the crystalline peaks at $2\theta = 9.77^\circ$ and $2\theta = 23.60^\circ$ signify the (001) and (002) crystalline

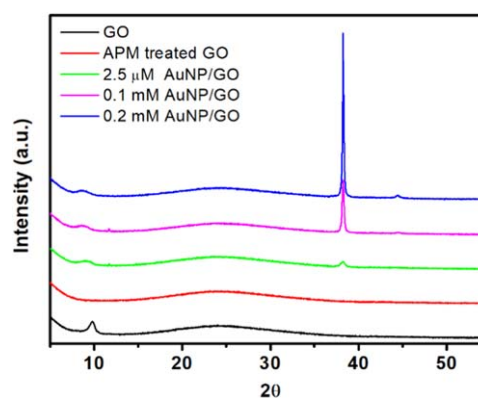


Figure 3. XRD spectra of pure GO, APM treated GO and AuNP/GO nanocomposites.

structures of GO, respectively [43]. After the APM treatment, the intensity of (001) peak was significantly reduced, indicating the reduction of oxygen-containing functionalities on GO [44]. This suggests the APM treatment has caused reduction of GO in aqueous mixtures containing HAuCl_4 . The finding is consistent with the previous study where GO was

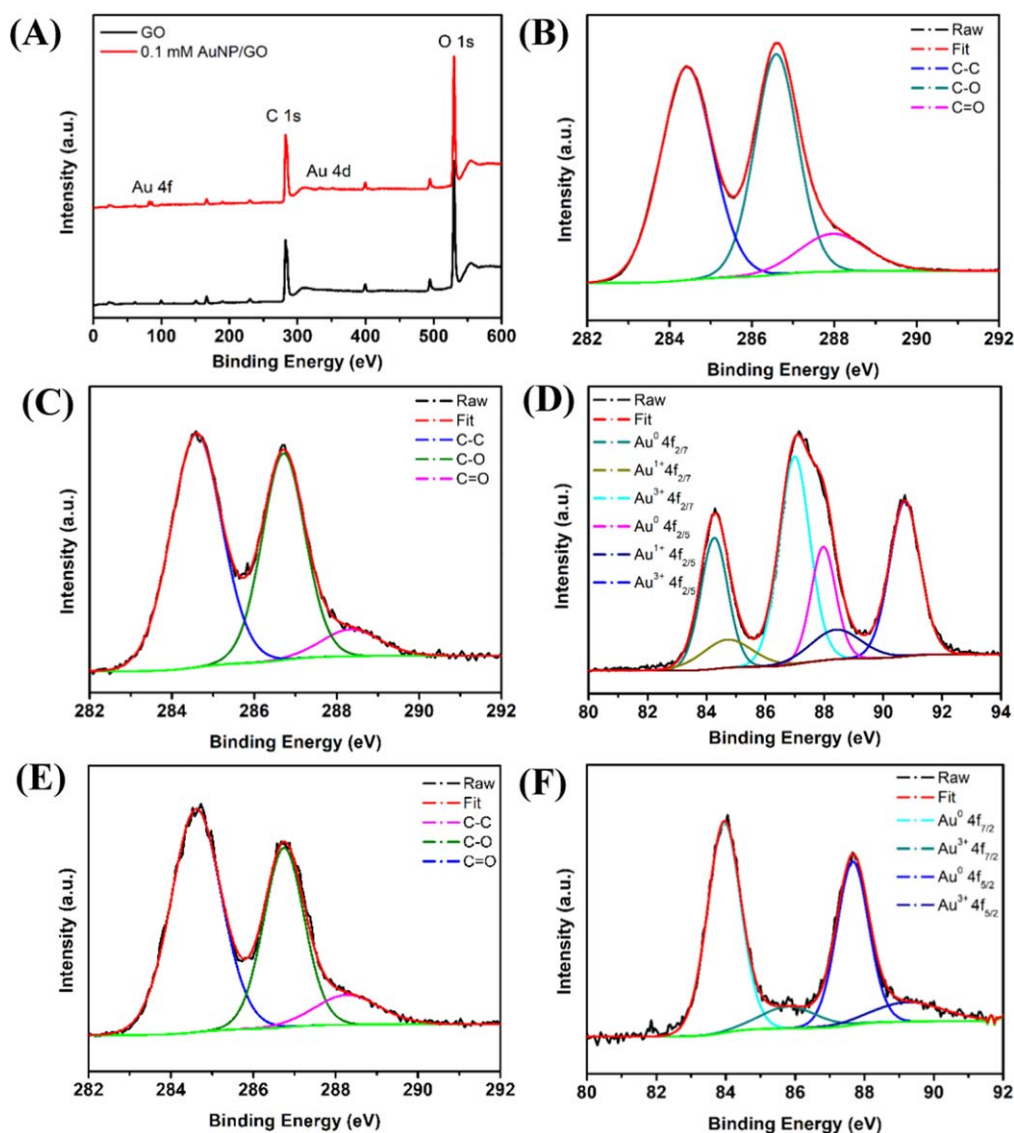


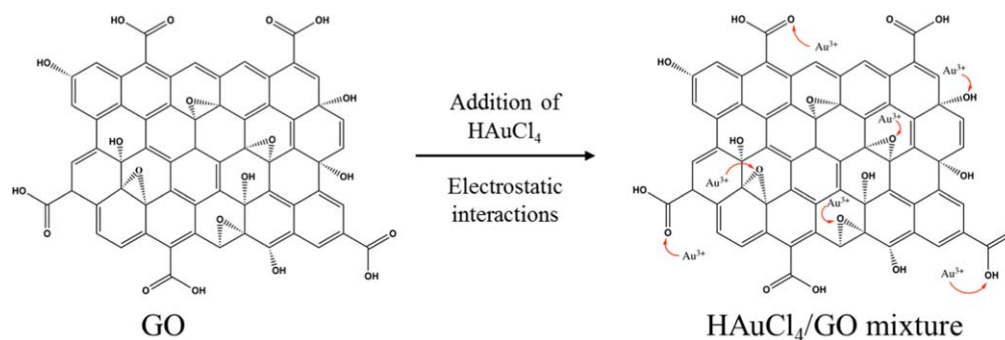
Figure 4. (a) Survey XPS spectra of GO and 0.1 mM AuNP/GO; (b) C 1s core peak of GO; (c) and (d) C 1s and Au 4f core peak of 0.1 mM HAuCl₄/GO; (d)–(e) C 1s and Au 4f core peak of 0.1 mM AuNP/GO.

Table 2. C 1s core peak analysis results for GO, 0.1 mM HAuCl₄/GO mixture and 0.1 mM AuNP/GO nanocomposites.

Samples		Carbon species			Au species		
		C–C	C–O	C=O	Au ¹⁺	Au ³⁺	Au ⁰
GO	BE (eV)	284.4	286.6	288.0	—	—	—
	Fraction (%)	47.9	41.0	11.1	—	—	—
0.1 mM HAuCl ₄ /GO	BE (eV)	284.6	286.7	288.3	84.7/88.4	87.0/90.7	84.2/87.9
	Fraction (%)	52.9	40.3	7.0	14.3	53.3	31.4
0.1 mM AuNP/GO	BE (eV)	284.6	286.7	288.3	84.9/88.8	—	84.0/87.7
	Fraction (%)	55.1	35.1	9.3	25.2	—	74.8

AMP treated in water only [2]. For AuNP/GO samples, the (001) peak of GO can still be observed in the XRD spectra. Comparing to the pure GO, the intensity of this peak also decreased, but to a lesser extent. Additionally, new peak at $2\theta = 38.2^\circ$ emerges, which correspond to the (111) facet of the face cornered cubic (fcc) gold nanostructures [45]. These results indicate that both Au ions and the GO surface oxygen-

functionalities have undergone reduction reaction during the APM process. There could be a competition between these two reduction processes, hence a lower degree of GO reduction is expected for the AuNP/GO sample (less reduced (001) GO peak intensity). With increasing initial HAuCl₄ concentration, the intensity of the $2\theta = 38.2^\circ$ peak significantly increases, suggesting that (111) facet is the



Scheme 2. The schematic of electrostatic interactions between Au^{3+} and oxygen-functionalities on the surface of GO.

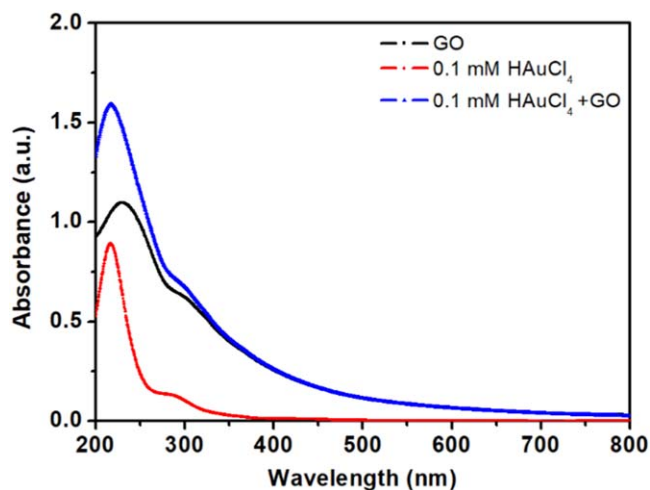
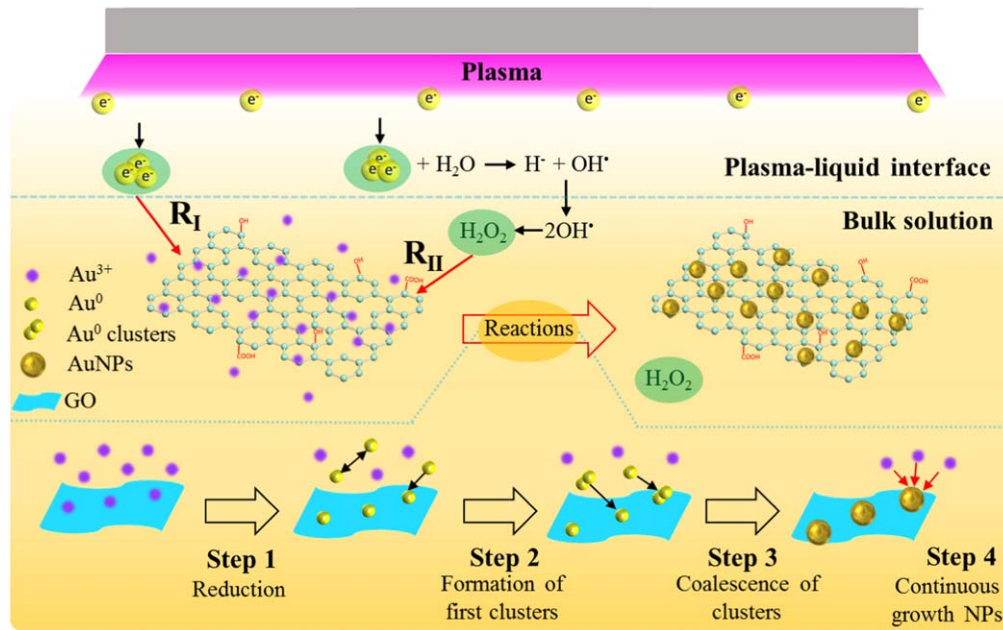


Figure 5. The UV-vis spectra of GO, 0.1 mM HAuCl_4 and 0.1 mM HAuCl_4/GO .

predominant AuNP growth orientation under the APM treatment [45]. The preferential growth of AuNPs along the (111) facet with increasing HAuCl_4 concentration suggest the crystal grown in these samples is dominated by the non-equilibrium kinetic growth regime [46, 47].

Figure 4(A) presents the survey XPS of pure GO and 0.1 mM AuNP/GO. In contrast to pure GO, a distinct Au 4f peak at binding energy (BE) around 83 eV (figure S3 in supporting information) can be found in the 0.1 mM AuNP/GO spectrum. The formation of AuNPs on the surface of GO resulted in a slightly increased C/O ratio in the survey spectra (from 1.83 for pure GO to 1.87 for 0.1 mM AuNP/GO). In order to develop more in-depth understanding of the AuNP-GO interfacial interaction, high-resolution XPS spectra of the C1s and Au 4f core peaks were further analysed for pure GO, 0.1 mM HAuCl_4/GO aqueous mixture, and 0.1 mM AuNP/GO nanocomposite. As is shown in figure 4(B), the C 1s core region of pure GO consist of three main components: 284.4 eV (C-C), 286.6 eV (C-O), and 288.0 eV (C=O) [48]; the fraction of each component is listed in table 2. The C 1s core peak in HAuCl_4/GO (figure 4(C)) consists of 284.6 eV (C-C), 286.7 eV (C-O), and 288.3 eV (C=O). Comparing to the C 1s peak of the pure GO sample, the BE of these signals have slightly shifted, indicating the change of their chemical environments. A possible reason for such change is the formation of Au-O-C bonds, as HAuCl_4 interacts with the GO

surface oxygen-functionalities [40]. The Au 4f core peak of the 0.1 mM HAuCl_4/GO mixture (figure 4(D)) can be deconvoluted into three doublets. The two doublets centred at BE of 84.7/88.4 eV and 87.0/90.7 eV can be correlated to the ionic Au states of the HAuCl_4 salt, Au^{1+} and Au^{3+} , respectively (table 2) [49–51]. A third doublet centred at 84.2/87.9 eV is also noticed, which signifies Au^0 state [52]. This could be due to the reduction of HAuCl_4 occurred during the XPS sample drying process, driven by the difference between the reduction potential of AuCl_4^- and the oxidation potential of GO [53]. However, this process is usually very slow, especially in the absence of external energy input (such as heating or sonication) [54], and the presence of AuNPs in the 0.1 mM HAuCl_4/GO mixture prior to APM treatment can be considered negligible in comparison to the AuNPs formed during the subsequent synthesis process. Figure 4(E) shows that after the APM treatment, the total fraction of oxygen-containing components (C-O and C=O) in the C 1s core peak of 0.1 mM AuNP/GO decreased from 52.1% to 44.9%. This reduction can be due to (i) the ability of APM to reduce the oxygen-containing groups of GO, as is supported by the XRD analysis earlier; and (ii) the APM induced AuNP formation on GO surface at the Au-O-C bonding sites. Figure 4(F) shows the Au 4f spectrum of the 0.1 mM AuNP/GO nanocomposite, where two doublets of the typical Au^{1+} peaks centred at the BE of 84.9/88.8 eV and the typical Au^0 peaks centred at the BE of 84.0/87.7 eV, respectively (table 2). Clearly, comparing to the Au 4f peak of 0.1 mM HAuCl_4/GO sample, the ionic state Au has gone through significant change during APM treatment. These results indicate the efficient reduction of gold precursor and formation of AuNP due to the APM treatment. In contrast to APM assisted synthesis of AuNPs only, the formation of AuNPs in the present work can be influenced by both the APM induced rich liquid chemistry and the presence of GO. When the HAuCl_4 was mixed with GO solution, the GO surface functional groups (-COOH, or O-C-O) will first interact with AuCl_4^- ions through electrostatic interaction, as is shown by scheme 2 [34]. Apart from the XPS analysis earlier, this interaction can also be evidenced by the UV-vis spectra shown in figure 5. The GO band (230 nm) in the UV-vis spectrum disappeared from the 0.1 mM HAuCl_4/GO aqueous mixture sample. Instead, a boarder AuCl_4^- band emerged at 216 nm, indicating the interfacial interaction between GO and HAuCl_4 . The



Scheme 3. Formation mechanism of AuNP/GO under the physical and chemical processes induced by APM.

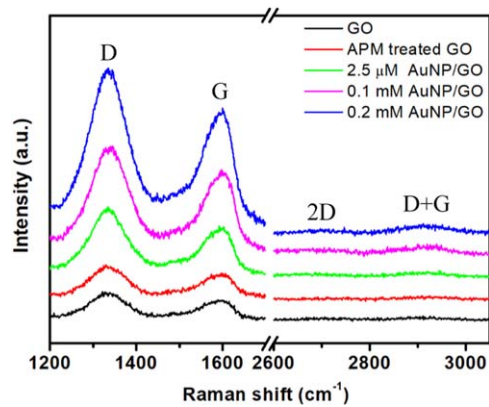


Figure 6. Raman spectra of GO, APM treated GO, and AuNP/GO nanocomposites.

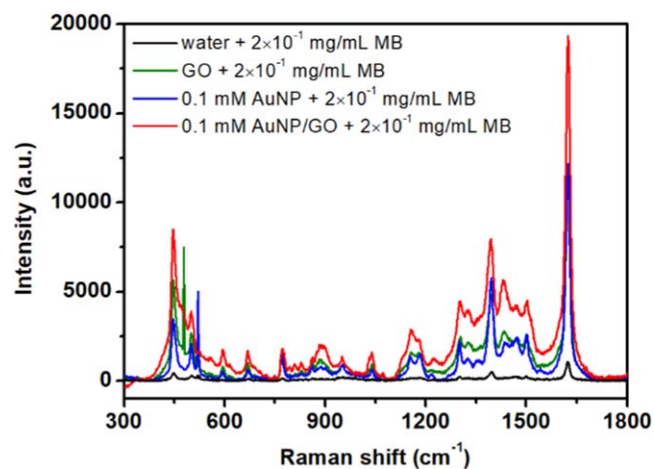
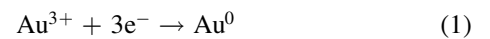


Figure 7. Raman spectra of GO, 0.1 mM AuNP, and 0.1 mM AuNP/GO for $2 \times 10^{-1} \text{ mg ml}^{-1}$ MB sensing; Pure MB was used as reference.

formation mechanism of AuNP/GO nanocomposites as a result of APM treatment has been illustrated in scheme 3. The solvated electrons (R_I in scheme 3) and H_2O_2 (R_{II} in scheme 3) are believed to be the two main species that trigger the initial reduction of the gold precursors [5, 8, 9, 12, 55]. When the mixture was subject to APM treatment, the AuCl_4^- ions anchored on the GO surface and any unbound free AuCl_4^- ions in the bulk solution were reduced into free Au^0 atoms through both R_I and R_{II} reaction pathways (step 1 in scheme 3). The associated half-cell reactions for R_I and R_{II} are:



It is worth pointing out that the reduction induced by the short-lived solvated electrons (equation (1)) is usually constrained at the plasma-liquid interfaces [9, 55], while the ability of H_2O_2 to diffuse into the bulk solution enable the reduction of the remaining gold precursors (AuCl_4^-) (equation (2)). The APM induced nucleation and subsequent NP growth in the present study is very much similar to the process seen in conventional wet chemistry; however, due to the APM induced reduction steps, the supply of the Au monomer is kinetically driven by the APM induced reaction products. That is, the initial growth of Au clusters is through the coalescence of Au atomic nuclei, and the subsequent growth of AuNPs arise from the coalescence of Au clusters at the cost of reduction in the number of clusters/NPs [56, 57]. In the presence of GO, on the other hand, the formation of first Au^0 clusters can take place on the Au–O–C bonding sites on the GO surface (or also in the bulk solution, depending on the HAuCl_4 precursor/GO ratio) (step 2). The as-formed Au^0 clusters further coalesce with others clusters to form stable seed AuNPs (step 3). In the event where residual Au ions are still present in the solution after step 3, the ions will be

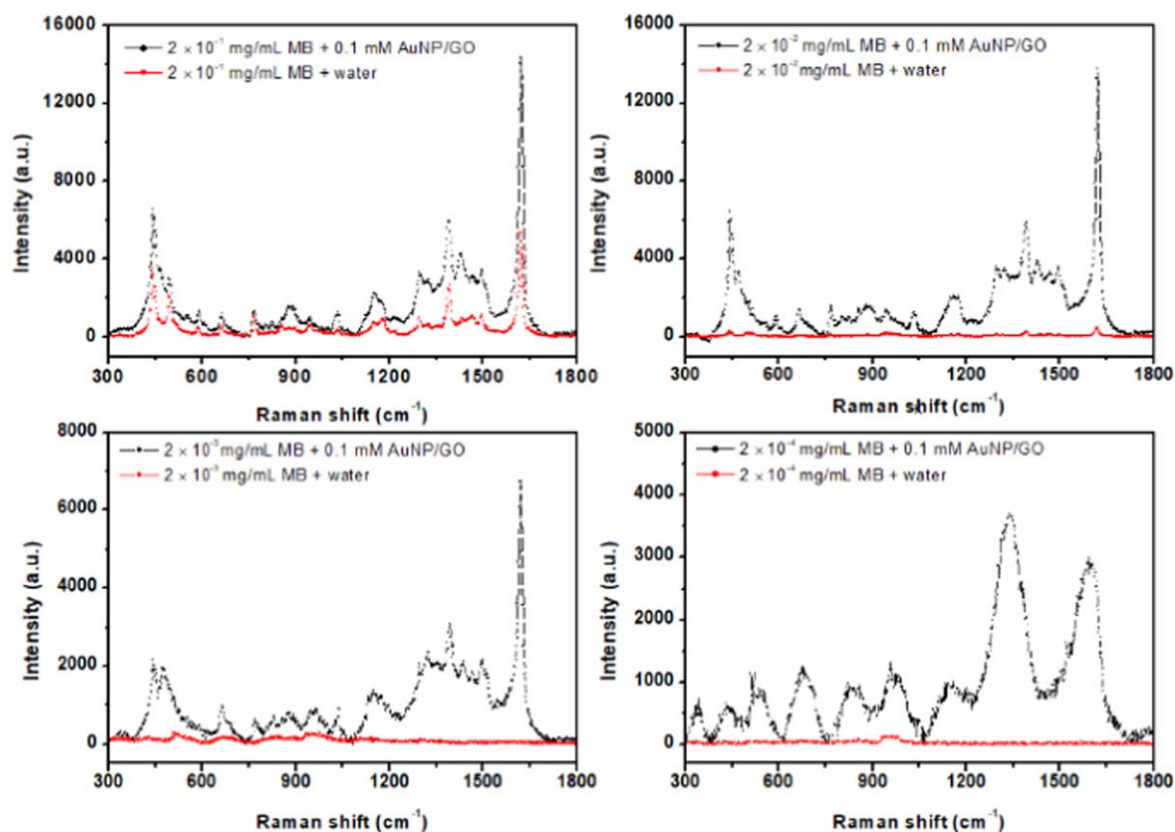


Figure 8. Raman spectra of 0.1 mM AuNP/GO for sensing MB with different concentrations.

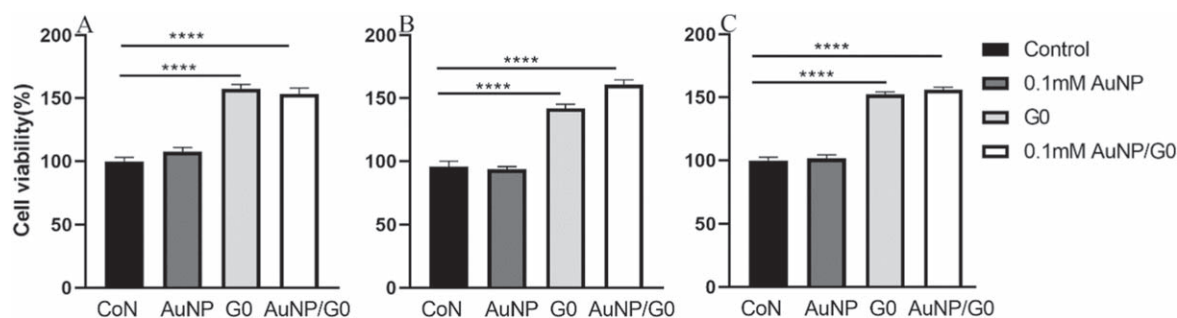


Figure 9. Cell viability of HeLa cell was measured by alamarBlue™ cell viability Assay after incubated with pure GO, 0.1 mM AuNP and 0.1 mM AuNP/GO for 24 h (A), 48 h (B), and 72 h (C), respectively. Data were presented as mean \pm S, E, and $N = 5$. One way ANOVA followed by Dunnett's multiple comparisons test. **** $p < 0.0001$.

attracted towards the seed AuNPs due to the presence of their surface electric double layer and the H_2O_2 within the bulk liquid will further reduce these ions into Au^0 as part of the continuous surface growth process (step 4) [8, 57, 58]. The AuNPs formed in the bulk solution could also be physically adsorbed onto the GO surface through the interactions between GO aromatic structures and d-orbitals of AuNPs via covalent attachment [40]. It should be noticed that the formation and growth of AuNPs will cease when AuCl_4^- ions within the precursor solution are depleted. For instance, in the 2.5 μM HAuCl_4/GO sample, the further growth of AuNP after the initial formation of Au clusters was not possible, due to the rapid depletion of AuCl_4^- ions at low precursor

concentration. Whereas for 0.1 and 0.2 mM AuNP/GO nanocomposites, there is more abundant supply of AuCl_4^- in the solution to sustain the growth of AuNPs until they reach their colloid stability. It should be noted that the morphology of the AuNPs can also be affected by the density and chemical nature of oxygenated groups on the GO surface [40].

The Raman scattering properties of our AuNP/GO nanocomposites have been investigated with pure GO and APM treated GO being the references, see figure 6. All samples feature a typical disordered band (D band at 1330 cm^{-1}) which represents the A_{1g} mode sp^2 hybridized carbon atoms in defects; and a typical graphene-like band (G band at 1596 cm^{-1}) which relates to the E_{2g} mode sp^3 -like

carbon atoms [59]. The D/G intensity ratio (I_D/I_G) of APM treated GO increased to 1.07, as compared to 1.04 for pure GO. The slight increase in the I_D/I_G ratio indicates that the APM treatment altered the structure of GO, due to the reduction of oxygen-containing groups [60]. Compared to pure GO and APM treated GO, AuNP/GO samples exhibit significantly stronger SERS at the D band and G band, and the intensity of the 2D peak ($\sim 2680\text{ cm}^{-1}$) and the D + G peak ($\sim 2911\text{ cm}^{-1}$) have also been enhanced. The enhancements of these Raman peaks can be attributed to the SPR oscillations of electrons on AuNPs under laser irradiation. Additionally, it is observed that the Raman signal intensifies for samples prepared from higher HAuCl_4 precursor concentrations. This can be related to the AuNPs size within the nanocomposites, as larger AuNPs normally possess higher SERS efficiency [16].

To evaluate the feasibility of our APM synthesized AuNP/GO nanocomposites for potential SERS biosensing, a commonly used aromatic molecule MB was chosen as a model probe [61, 62]. Figure 7 presents the Raman scattering spectrum of MB only (control) and the SERS spectra of MB on pure GO, 0.1 mM AuNP, and 0.1 mM AuNP/GO nanocomposites, respectively. It is noticed that the Raman signal (based on the characteristic band at 1625 cm^{-1}) of MB is negligible in the MB only sample. When GO or 0.1 mM AuNP were used as SERS substrates, the MB SERS signals are intensified significantly. The enhancement seen in these two samples is due to the charge transfer between MB and the substrate via two different SERS enhancement mechanisms: (i) CM due to the π - π stacking between MB and GO, and (ii) EM due to the electrostatic interaction between MB and AuNPs [30, 63, 64]. When 0.1 mM AuNP/GO was used as the SERS substrate, the signal was further enhanced, due to the combined effects of CM and EM. In order to quantitatively determine the SERS sensitivity of our AuNP/GO nanocomposites, MB solutions with different concentrations were tested. Figure 8 shows that the Raman signal of MB only sample can be hardly detected when the concentration is lower than $1 \times 10^{-1}\text{ mg ml}^{-1}$. However, the use of 0.1 mM AuNP/GO significantly enhanced the characteristic peak signal (1625 cm^{-1}) and the detection limit can reach as low as $1 \times 10^{-3}\text{ mg ml}^{-1}$.

The biocompatibility of SERS substrate material is of particular importance for bio-related SERS applications [65]. In this work, the cytotoxicity of 0.1 mM AuNP/GO was evaluated *in vitro* using HeLa cell using alamarBlue™ cell viability Assay. The cytotoxicity of the pure GO and the 0.1 mM AuNP were used as reference. Results show that all samples are highly biocompatible after incubation of 24 h (figure 9(A)), 48 h (figure 9(B)), and 72 h (figure 9(C)). Both GO and 0.1 mM AuNP/GO show comparable biocompatibility, as well as ability to further enhance the cell proliferation comparing to the 0.1 mM AuNP sample. These preliminary results demonstrate that our AuNP/GO nanocomposites are highly biocompatible and may be considered for biosensing applications and beyond.

Conclusion

In summary, we demonstrated a rapid and facile single step APM based approach for synthesizing AuNP/GO nanocomposites. The reactive species generated through APM-liquid interaction are responsible for the formation of the AuNP-GO nanocomposites within the complicated multi-phase reaction system consisting of gas, liquid and solid nanomaterials. The as-synthesized AuNP/GO nanocomposites exhibited excellent biocompatibility and has been demonstrated for SERS sensing applications where high detection sensitivity (probe molecule concentration as low as $1 \times 10^{-3}\text{ mg ml}^{-1}$) has been achieved.

Acknowledgments

The authors would like to acknowledge the Engineering and Physical Sciences Research Council (EPSRC) for funding support (EP/P00394X/1 and EP/M024938/1). This research has also been supported from the European Union's Horizon 2020 research and innovation programme under the Marie Skłodowska-Curie grant agreement No. 722717 (OCUTHER). Daye Sun thanks the China Scholarship Council (CSC) for the financial support.

ORCID iDs

Daye Sun  <https://orcid.org/0000-0002-8422-8381>
Li Zhang  <https://orcid.org/0000-0002-1832-6290>
Brian G Falzon  <https://orcid.org/0000-0002-3613-2924>
Davide Mariotti  <https://orcid.org/0000-0003-1504-4383>
Paul Maguire  <https://orcid.org/0000-0002-2725-4647>
Heping Xu  <https://orcid.org/0000-0003-4000-931X>
Dan Sun  <https://orcid.org/0000-0002-5100-2749>

References

- [1] Mariotti D and Sankaran R M 2010 *J. Phys. D: Appl. Phys.* **43** 323001
- [2] McKenna J, Patel J, Mitra S, Sojn N, Švrček V, Maguire P and Mariotti D 2011 *Eur. Phys. J. Appl. Phys.* **56** 24020
- [3] Mariotti D, Patel J, Nemcova L, Maguire P, Grahamand W G and Mariotti D 2012 *Plasma Process. Polym.* **9** 1074–85
- [4] Bruggeman P J *et al* 2016 *Plasma Sources Sci. Technol.* **25** 053002
- [5] Bratescu M A, Cho S P, Takai O and Saito N 2011 *J. Phys. Chem. C* **115** 24569–76
- [6] Huang X Z, Zhong X X, Lu Y, Li Y S, Rider A E, Furman S A and Ostrikov K 2013 *Nanotechnology* **24** 095604
- [7] Du C and Xiao M 2014 *Sci. Rep.* **4** 7339
- [8] Patel J, Němcová L, Maguire P, Graham W G and Mariotti D 2013 *Nanotechnology* **24** 245604
- [9] Maguire P, Rutherford D, Macias-Montero M, Mahony C, Kelsey C, Tweedie M, Pérez-Martin F, McQuaid H, Diver D and Mariotti D 2017 *Nano Lett.* **17** 1336–43
- [10] Ni C *et al* 2018 *Green Chem.* **20** 2101

- [11] Wang R, Zuo S, Zhu W, Zhang J and Fang J 2014 *Plasma Process. Polym.* **11** 448–54
- [12] Yan T, Zhong X, Rider A E, Lu Y, Furman S A and Ostrikov K K 2014 *Chem. Commun.* **50** 3144–7
- [13] Zhang R C, Sun D, Zhang R, Lin W F, Macias-Montero M, Patel J, Askari S, McDonald C, Mariotti D and Maguire P 2017 *Sci. Rep.* **7** 46682
- [14] Nolan H, Sun D, Falzon B G, Maguire P, Mariotti D, Zhang L and Sun D 2019 *Plasma Process. Polym.* **16** 1800128
- [15] Nolan H et al 2018 *Plasma Process. Polym.* **15** 1800112
- [16] Sun D, McLaughlan J, Zhang L, Falzon B G, Mariotti D, Maguire P and Sun D 2019 *Langmuir* **35** 4577–88
- [17] Zhu Y, Murali S, Cai W, Li X, Suk J W, Potts J R and Ruoff R S 2010 *Adv. Mater.* **22** 3906–24
- [18] He M, Chen X, Guo Z, Qiu X, Yang Y, Su C, Jiang N, Li Y, Sun D and Zhang L 2019 *Comput. Sci. Tech.* **174** 194–201
- [19] Chen C, Sun X, Pan W, Hou Y, Liu R, Jiang X and Zhang L 2018 *ACS Sustain. Chem. Eng.* **6** 3862–9
- [20] Ma X, Qu Q, Zhao Y, Luo Z, Zhao Y, Ng K W and Zhao Y 2013 *J. Mater. Chem. B* **1** 6495–500
- [21] Saravanan S et al 2018 *Sci. Rep.* **8** 15069
- [22] Liu J, Ma Q, Huang Z, Liu G and Zhang H 2018 *Adv. Mater.* **31** 1800696
- [23] Turcheniuk K, Boukherroub R and Szunerits S 2015 *J. Mater. Chem. B* **3** 4301–24
- [24] Jensen L, Aikens C M and Schatz G C 2008 *Chem. Soc. Rev.* **37** 1061–73
- [25] Yu X, Cai H, Zhang W, Li X, Pan N, Luo Y, Wang X and Hou J G 2011 *ACS Nano* **5** 952–8
- [26] Wang P, Liang O, Zhang W, Schroeder T and Xie Y H 2013 *Adv. Mater.* **25** 4918–24
- [27] Tao Y, Lin Y, Huang Z, Ren J and Qu X 2013 *Adv. Mater.* **25** 2594–9
- [28] Huang J, Zong C, Shen H, Liu M, Chen B, Ren B and Zhang Z 2012 *Small* **8** 2577–84
- [29] Lu G, Li H, Liusman C, Yin Z, Wu S and Zhang H 2011 *Chem. Sci.* **2** 1817–21
- [30] Fu W L, Zhen S J and Huang C Z 2013 *Analyst* **138** 3075–81
- [31] Hu C, Rong J, Cui J, Yang Y, Yang L, Wang Y and Liu Y 2013 *Carbon* **51** 255–64
- [32] Wang Q, Li Q, Yang X, Wang K, Du S, Zhang H and Nie Y 2016 *Biosens. Bioelectron.* **77** 1001–7
- [33] Iliut M, Leordean C, Canpean V, Teodorescu C M and Astilean S 2013 *J. Mater. Chem. C* **1** 4094–104
- [34] Goncalves G, Marques P A A P, Granadeiro C M, Nogueira H I S, Singh M K and Grácio J 2009 *Chem. Mater.* **21** 4796–802
- [35] Li Y, Yang J, Zhou Y, Zhao N, Zeng W and Wang W 2017 *Colloids Surf. A* **512** 93–100
- [36] Li Y, Yang J, Zhou Y Z, Zhong T, Zheng S H and Zeng W W 2016 *Mon. hefte Chem.* **147** 677–83
- [37] Huang J, Zhang L, Chen B, Ji N, Chen F, Zhang Y and Zhang Z 2010 *Nanoscale* **2** 2733–8
- [38] Fan Z, Kanchanapally R and Ray P C 2013 *J. Phys. Chem. Lett.* **4** 3813–8
- [39] Hu Y, Lu L, Liu J and Chen W 2012 *J. Mater. Chem.* **22** 11994–2000
- [40] Hernández-Sánchez D, Villabona-Leal G, Saucedo-Orozco I, Bracamonte V, Pérez E, Bittencourt C and Quintana M 2018 *Phys. Chem. Chem. Phys.* **20** 1685–92
- [41] Matsumura Y and Ananthaswamy H N 2004 *Toxicol. Appl. Pharmacol.* **195** 298–308
- [42] Haiss W, Thanh N T K, Aveyard J and Fernig D G 2007 *Anal. Chem.* **79** 4215–21
- [43] McAllister M J et al 2007 *Chem. Mater.* **19** 4396–404
- [44] Huang H H, De Silva K K H, Kumara G R A and Yoshimura M 2018 *Sci. Rep.* **8** 6849
- [45] Li C C, Chen L B, Li Q H and Wang T H 2012 *CrystEngComm* **14** 7549–51
- [46] Evans J E, Jungjohann K L, Browning N D and Arslan I 2011 *Nano Lett.* **11** 2809–13
- [47] Cheong S, Watt J D and Tilley R D 2010 *Nanoscale* **2** 2045–53
- [48] Otari S V, Kumar M, Anwar M Z, Thorat N D, Patel S K S, Lee D, Lee J H, Lee J K, Kang Y C and Zhang L 2017 *Sci. Rep.* **7** 10980
- [49] Yang E, Chou H, Tsumura S and Nagatsu M 2016 *J. Phys. D: Appl. Phys.* **49** 185304
- [50] Minicò S, Scirè S, Crisafulli C and Galvagno S 2001 *Appl. Catal. B* **34** 277–85
- [51] Goguet A, Ace M, Saih Y, Sa J, Kavanagh J and Hardacre C 2009 *Chem. Commun.* **0** 4889–91
- [52] Boyen H G et al 2002 *Science* **297** 1533–6
- [53] Zhang N, Qiu H, Liu Y, Wang W, Li Y, Wang X and Gao J 2011 *J. Mater. Chem.* **21** 11080–3
- [54] Li X R, Li X L, Xu M C, Xu J J and Chen H Y 2014 *J. Mater. Chem. A* **2** 1697–703
- [55] Rumbach P, Bartels D M, Sankaran R M and Go D B 2015 *Nat. Commun.* **6** 7248
- [56] Polte J, Erler R, Thünemann A F, Sokolov S, Ahner T T, Rademann K, Emmerling F and Kraehnert R 2010 *ACS Nano* **4** 1076–82
- [57] Polte J 2015 *Cryst. Eng. Comm.* **17** 6809–30
- [58] Wuihshick M, Birnbaum A, Witte S, Sztucki M, Vainio U, Pinna N, Rademann K, Emmerling F, Kraehnert R and Polte J 2015 *ACS Nano* **9** 7052–71
- [59] Malard L M, Pimenta M A, Dresselhaus G and Dresselhaus M S 2009 *Phys. Rep.* **473** 51–87
- [60] Moon I K, Lee J, Ruoff R S and Lee H 2010 Reduced graphene oxide by chemical graphitization *Nat. Commun.* **1** 73–9
- [61] Yilmaz M, Babur E, Ozdemir M, Giesecking R L, Dede Y, Tamer U, Schatz G C, Facchetti A, Usta H and Demirel G 2017 *Nat. Mater.* **16** 918–24
- [62] Reguera J, Langer J, Jiménez De Aberasturi D and Liz-Marzán L M 2017 *Chem. Soc. Rev.* **46** 3866–85
- [63] Hao Q, Wang B, Bossard J A, Kiraly B, Zeng Y, Chiang I K, Jensen L, Werner D H and Huang T J 2012 *J. Phys. Chem. C* **116** 7249–54
- [64] Huh S, Park J, Kim Y S, Kim K S, Hong B H and Nam J M 2011 *ACS Nano* **5** 9799–806
- [65] Samanta A, Jana S, Das R K and Chang Y T 2014 *RSC Adv.* **4** 12415–21